Determination of Primary Mineral Content and Calcium Sources in Forest Soils using Electron Probe Microanalysis Mapping and Cluster Analysis

Scott W. Bailey*
USDA Forest Service
Northern Research Station
234 Mirror Lake Road
North Woodstock, NH 03262

Donald S. Ross
Univ. of Vermont
Dep. of Plant and Soil Science
Burlington, VT 05405-1737

Nico Perdrial
Univ. of Vermont
Dep. of Geology
Burlington, VT 05405-1737

Michael Jercinovic
Univ. of Massachusetts
Dep. of Geosciences
Amherst, MA 01003

Jeffrey Webber
Stockton Univ.
Dep. of Geology
Galloway, NJ 08205-9441

Rebecca Bourgault
Bloomsburg Univ. of Pennsylvania
Dep. of Environmental, Geographical, and Geological Sciences
Bloomsburg, PA 17815

Although mineral dissolution is a fundamental soil forming process, primary mineral content of soils is rarely inventoried or quantified. Concerns about maintenance of forest soil nutrient stocks require better mineralogic data. In particular, to understand recovery from Ca losses induced by acid deposition and sustainability of intensive forest harvest, better inventory of primary Ca minerals is needed. We developed a method based on electron probe micro-analysis to quantify primary mineral concentrations in soil. Samples analyzed from three sites in the glaciated northeastern United States spanned a bulk Ca concentration of 0.03 to 0.94%. Plagioclase was the dominant Ca-bearing mineral at two sites while apatite was the only Ca-bearing mineral found in all three samples and was the dominant calcium source at one site. A variety of other Ca silicate minerals were found in trace amounts. Electron probe microanalysis (EPMA) proved more sensitive in detecting minor and trace Ca bearing minerals than standard XRD procedures. The Ca-bearing minerals detected by EPMA matched those expected based on the lithologic composition of the glacial till and were consistent with measured bulk soil Ca content by lithium-borate fusion. Taking into account the Ca concentration in each mineral and each mineral's abundance in the sample, this inventory provided a complete accounting of Ca sources.

Abbreviations: EDS, energy dispersive spectrometry; EPMA, electron probe microanalysis; HB, Hubbard Brook Experimental Forest; SEM, scanning electron microscopy; SR, Sleepers River Research Watershed 9; WN, Winnisook watershed; XRD, x-ray diffraction.

Core Ideas

- **Electron probe microanalysis mapping successfully quantified primary mineral content.**
- **X-ray diffraction did not detect trace minerals or identify solid solution minerals.**
- **Accurate inventory of primary minerals is needed for soil process studies.**

Primary mineral weathering is a fundamental process in soil development as the main consumer of acidity (Binkley and Richter, 1987) and as the producer of secondary clays and less crystalline materials that contribute to moisture retention and cation exchange. In addition, many required nutrients, such as Ca, Mg, K, P, etc., are released to soluble form by dissolution of primary minerals, the major source of such nutrients for maintenance of life. Yet, the primary mineral content of soil is often not well studied or inventoried. The US soil taxonomic system considers mineralogy at the family level, focusing on secondary minerals formed in the weathering environment as indicators of the mechanisms and degree of soil formation. Less attention is paid to the primary mineral content of soils, with less weathered soils dominated by primary minerals inherited from parent material lumped into the mixed mineralogy family (Soil Survey Staff, 2014). Yet, the primary mineral composition is a first order control on weathering processes, with minerals commonly found in soil varying widely in their content of nutrient elements and over six orders of magnitude in dissolution rate (Brantley, 2008).

Quantification of mineral weathering fluxes is of paramount importance for understanding responses of ecosystems to anthropogenic disturbances. Critical load formulations, used to determine levels of acid deposition detrimental to forest and

Soil Sci. Soc. Am. J. 83:1830–1841
doi:10.2136/sssaj2019.07.0231
Received 29 July 2019.
Accepted 19 Sept. 2019.
*Corresponding author (scott.bailey@usda.gov).

aquatic ecosystems, are based on the balance between base cation release via mineral weathering and losses via biomass uptake and removal, and hydrologic leaching (Pardo, 2010). The sustainability of forest productivity and harvesting is governed by this same balance (Federer et al., 1989; Vadeboncoeur et al., 2014). While biomass growth, harvest removals and hydrologic losses are relatively easily monitored, mineral weathering cannot be directly measured and must be estimated by indirect means, such as the difference in a mass balance equation (Likens et al., 1996), using isotopic or geochemical proxies (Bailey et al., 1996; Velbel and Price, 2007) or via process modeling (Kolka et al., 1996; Futter et al., 2012). These approaches are informed, and limited, by an accurate inventory of soil mineral content as the foundation for realistic estimates of mineral weathering flux.

Common approaches to estimate soil mineral content include analysis of bulk element composition by acid digestion, fusion, or x-ray fluorescence, and use of a model to convert chemical composition into modal mineral content, or by direct determination of mineral content by x-ray diffraction (XRD). The former method depends on a development of a model to translate element abundance to mineral composition, based on typical mineral content determined for a relatively small number of samples (Sverdrup and Warfvinge, 1993). The limitation of this approach is that there are multiple possible mineral contents for a given soil bulk composition and the model relating chemical and mineral composition may not be applicable outside of a narrowly defined or relatively uniform geologic region where it was initially developed. The latter method is limited by the detection and quality of diffraction patterns, which may be poor due to damaged mineral crystal lattices due to partial dissolution, preferential orientation of minerals in the preparation, and low abundance of the most important (i.e., weathering-susceptible) minerals compared to the dominant quartz content of most soils. Neither method can give the exact stoichiometry of common solid-solution minerals, such as hornblende or biotite, which have one or more coupled element substitutions in their crystal structure, resulting in a wide range of possible chemical compositions. A more direct and automated approach is needed to provide a ready and accurate inventory of soil mineralogy. Determining exact mineral compositions with electron probe microanalysis (EPMA) has been shown to have a strong effect on modeled weathering rates (Casetou-Gustafson et al., 2019) but to date, this technique has not been used to determine overall soil mineral content.

In particular, inventories of calcium (Ca) bearing minerals are especially needed, as Ca is the major nutrient hypothesized to be most susceptible to depletion from forest soils in regions affected by atmospheric acid deposition and forest harvesting (Federer et al., 1989). Such depletion has been inferred using mass balance approaches (Bailey et al., 1996; Likens et al., 1996), directly measured via soil resampling (Bailey et al., 2005), and induced by experimental acid additions (Fernandez et al., 2003). As acid deposition levels have fallen in recent years, recovery of soils from Ca depletion is incomplete. It is unknown how long recovery will take due to uncertainty in rates of replenishment of Ca supplies via mineral weathering (Lawrence et al., 2015). Similarly, response of forest soils to intensive harvesting is poorly understood and limited by knowledge of the identity of Ca-bearing minerals and their amount and location within soil profiles (Bailey et al., 2003).

We sought to determine the mineral content, especially the chemistry and content of Ca-bearing minerals, in representative forest soils of the glaciated northeastern United States, a region impacted by relatively high rates of atmospheric acid deposition where Ca depletion of forest soils has been an ongoing issue of management and policy concern. We chose three study sites based on a range of lithologic composition of glacial drift soil parent material, hypothesized to span the range of Ca content of northeastern US forest soils, and likely containing a variety of Ca-bearing soil minerals. Inventory of soil mineral content and Ca-bearing phases was made by EPMA of multiple elements of soil thin sections, followed by image analysis to create maps of mineral content of soil thin-sections. Results were confirmed with both petrographic and scanning electron microscopy and compared to results from conventional x-ray diffraction.

METHODS

Study Sites and Samples

Three regional ecosystem monitoring sites (www.nercscience.org) spanning a range of bedrock geology, soil parent material lithology, and Ca status were chosen for investigation. All three sites are covered by relatively mature northern hardwood forest dominated by American beech (*Fagus grandifolia*), yellow birch (*Betula alleghaniensis*) and sugar maple (*Acer saccharum*) and have soils developed in Wisconsinan glacial till. Sleepers River Research Watershed 9 (SR) is a headwater catchment in northern Vermont with relatively Ca-rich soils (Park et al., 2008) and bedrock primarily composed of the calcareous Waits River Formation (Hall, 1959) (Table 1). Hubbard Brook Experimental Forest (HB) includes a series of headwater catchments in central New Hampshire with relatively Ca-poor soils (Park et al., 2008) developed in primarily granitic glacial drift (Bailey et al., 2003). Our sampling site was just west of Watershed 6 in the northern hardwood plot used as a reference site for other biogeochemical studies (Palmer et al., 2004). The Winnisook watershed (WN) in the Catskill Mountains of southeastern New York is the headwater catchment used in a number of nested catchment biogeochemistry studies in the Neversink River drainage, a primary water supply of New York City (McHale et al., 2017). Bedrock at WN is primarily composed of sandstone and conglomerate and soils have very low Ca levels (Johnson et al., 2000; Ver Straeten, 2013).

At each site, a soil sampling pit was hand-dug to a depth of about 1 m, usually about 0.2 m into the relatively unweathered C-horizon. All major horizons were described and sampled from the pit face. Lithologic composition of the glacial till was determined by collecting at least 100 gravels 2 to 7.5 cm across collected from the soil pit, cleaned in an ultrasonic bath, and visually identified via comparison to reference samples from locally mapped bedrock units. Such results were previously published by Bailey et al. (2003) for eight pits at HB. We collected, cleaned, and identi-

Table 1. Site and sample description. Soil taxonomy refers to the classification of the sampled pedon. Sites are Sleepers River Research Watershed 9 (SR) in northern Vermont, Hubbard Brook Experimental Forest (HB) in central New Hampshire, and Winnisook watershed (WN) in southeastern New York.

	SR	HB	WN
Location	44°30′ N, 72°10′ W	43°57′ N, 71°44′ W	42°00′ N, 74°24′ W
Elevation, m	594	750	922
Soil taxonomy	Coarse-loamy, mixed, semiactive, frigid Aquic Humudept	Coarse-loamy, isotic, frigid Aquic Haplorthod	Coarse-loamy, isotic, frigid Typic Haplorthod
Horizon sampled	Bw	Bhs	Cd
Sample depth, cm	21–26	18–23	115–120
Soil Texture	loam	sandy loam	sandy loam
Sand, %	45	67	65
Coarse silt, %	14	8	7
Fine silt, %	31	19	22
Clay, %	10	6	6

fied gravels from four pits from SR and three pits from WN. Based on the rock lithologies identified in the gravel samples, and mineralogic composition of local rocks reported in the literature, we developed a list of minerals we expected to find in the soil.

For detailed mineralogic determination, we focused on lower B or C horizon samples to minimize weathering loss of less common, more easily weathered minerals, thus maximizing the variety of minerals we were likely to detect. One sample from each site was chosen to develop the methodology. Samples of approximately one liter in volume were air-dried, sieved to <2 mm, mixed thoroughly and quantitatively separated by riffling into subsamples for storage and further analysis. One set of subsamples was prepared for electron probe microanalysis (EPMA) by epoxy impregnation under vacuum, mounting on a standard 27 mm by 46 mm glass slide, thin sectioning and polishing to a thickness of 30 μm. Exchangeable Ca was determined by extraction in 1 *M* NH_4Cl via a mechanical vacuum extractor (Blume et al., 1990). A powdered subsample was fused with lithium borate. The resulting glass bead was dissolved in dilute HCl. Cations in salt extraction and major elements in fusion solutions were analyzed on a Varian Vista ICP at the Forestry Sciences Lab, Durham NH. As an additional soil characterization measure, particle size distribution was determined by the hydrometer method after dispersion in sodium hexametaphosphate (Day, 1965).

EPMA Mapping

Electron Probe Wavelength Dispersive Spectroscopic Micro-Analysis (EPMA) was performed at the University of Massachusetts Department of Geosciences Electron Microprobe/SEM Facility on a Cameca SX50 electron microprobe with five wavelength dispersive spectrometers. Mapping proceeded in an automated mode with stage rastered mapping on the full section (~20 mm by 17 mm) in 30 by 30 μm pixels. The five spectrometers were used to measure the distribution of Ca, P, Si, Al and Fe (Fig. 1). Each thin section map contained an average of 370,000 pixels and required 420 min to complete.

Occasionally geometrical variation correction is needed because of defocusing of the spectrometer as a function of stage position, and this was the case with the SR sample. As x-ray count rates can vary depending on how flat the sample surface is, a small change in stage Z position as mapping progresses can yield a significant decrease in x-ray intensity as the sample deviates from perfect x-ray focus. The elements Si, Al, and Mg are more susceptible to this defocusing and commonly produce systematic variations in counts across a map. The general approach to correct for systematic variation used control points of assumed constant composition for each element in the system. For example, if a sample has a matrix of plagioclase grains that are not highly zoned in composition, the cores of grains across the map can be used to correct for Al + Si ± Na ± Ca. A script written in the statistical computing environment R (R Core Team, 2013) read through the locations of control points and extracted pixel values for each element of interest from the raw wavelength dispersal spectrometry (WDS) maps. Noise in the control points was reduced by averaging the values of the eight surrounding pixels

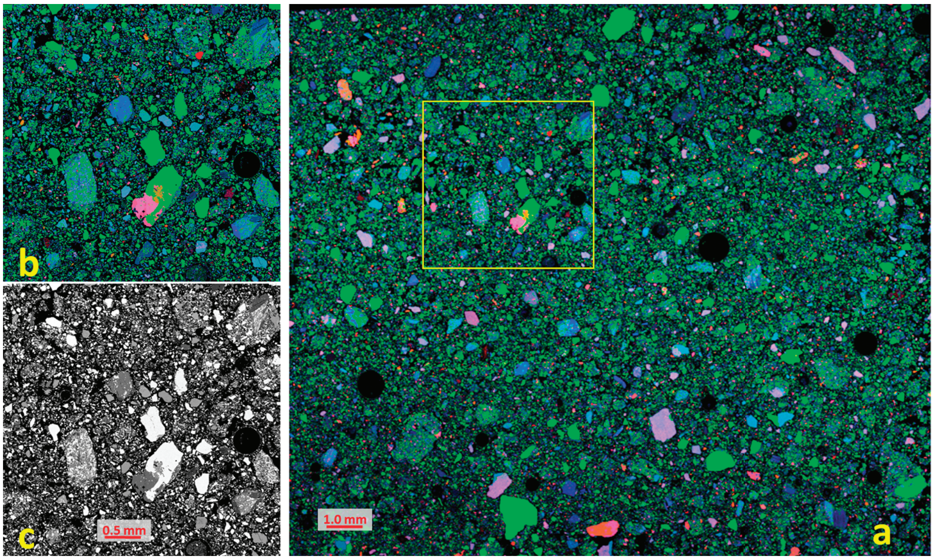

Fig. 1. False color uncorrected elemental maps of Sleepers River Bw sample showing (a) entire slide (30 by 30 μm pixels) with Si (green), Al (blue), and Ca (red); (b) enlargement of a portion (10 by 10 μm pixels) of the area indicated by the yellow square, and (c) SEM image of the same area.

in addition to the selected pixel. The pixel coordinates (XY) and values (Z) were then used to fit a local polynomial regression across the entire mapping area. This was completed with the loess function in the R stats base package based on Cleveland et al. (1992). The local polynomial regression was then used to predict values for every pixel. The fitted surface was used to normalize the corresponding raw WDS map. The result of the correction produces WDS maps for each element analyzed that do not display significant spatial variation in count intensity (Supplemental Fig. S1).

To convert EPMA raw counts to elemental concentrations, two smaller areas (5 mm by 5 mm) in the sample from SR were mapped with EPMA at a finer scale (10 by 10 μm; see Supplemental Fig. S2) and then elemental point counts were taken at areas of interest using energy dispersive spectrometry (EDS). Elements quantified were P, Si, Al, Ca and Fe (along with S, Ti, Cr, Mg, Mn, Na and K to aid with mineral identification). After locating each point on the full section map, average elemental counts were obtained from 8 to 90 pixels in the surrounding area. The number of pixels used was contingent on the variability of the counts around the quantification point, using more pixels in the case of relatively large homogeneous minerals. In a few cases, counts were too variable to determine a reliable average and these points were not used. Simple least squares fits were developed for Si, Al and Fe with R^2 between 0.98–1.00. Calcium was calculated with a linear formula below about 1% Ca and a quadratic formula at higher counts. Phosphorus was estimated by assuming that a 7-pixel area with the highest P counts in an apatite grain had the ideal concentration of 18.43% P and that lower counts were linearly proportional. These formulas were then applied to the mean elemental counts for each cluster, as described below, to provide elemental concentrations that were then used in mineral identification.

Cluster Analysis and Calculation of Mineral Abundance

Multispec software (Biehl and Landgrebe, 2002) was used to combine the full section element maps and create false color images. Comprehensive instructions provided by Lydon (2005) were used to process the data and identify specific minerals. Initial efforts focused on 'training' the maps by identifying areas of known minerals and allowing the software to identify the remaining pixels based on patterns in those areas. This did not produce satisfactory maps, probably because of the high number of soil particle edge pixels found in each map; much higher than a thin section of rock because of the small size of soil particles relative to the electron beam and the intervening void space. Instead, cluster analysis was performed using Multispec and the five element maps for each thin section. For the three maps presented here, a simple single pass cluster analysis was used for SR and WN whereas the iterative 'ISODATA' approach was used for HB because single pass was not providing satisfactory results. All approaches used a minimum cluster size of six and the output created between 43 and 66 clusters. Calculated percent content of the mapped elements for each cluster was derived from the cluster mean counts and the fitting equations described above. Using this information, specific minerals were assigned to clusters and, when possible, clusters were grouped according to this identification. Rules for mineral identification were established and used as a first step in the process (Supplemental Table S1). The volume percent occurrence of each identified mineral phase was calculated by dividing its number of areal pixels by the total non-void space. Non-void space was the total space minus the sum of void pixels (elemental content greater than ~10%) and void space within pixels calculated if the sum of the elements converted to oxides was <85%. Volume was converted to a mass percent occurrence by correcting for the specific gravity of each mineral, obtained from Deer et al. (2013).

Refinement of the assignment of mineral identifications occurred in an iterative process with (i) more EPMA mapping accompanied by energy dispersive spectroscopy (EDS) elemental quantification, and (ii) optical identification of the larger mineral particles with a petrographic microscope. Further SEM/EDS was performed at the University of Vermont Medical Imaging Facility using a JEOL 6060 scanning electron microscope with an Oxford Instruments EDS. Both point counts and small maps were obtained from a variety of areas to confirm mineral identification. Phase maps were prepared with Oxford's INCA Suite version 4.15 (Oxford Instruments Analytical Ltd., Abingdon, Oxfordshire).

X-ray Diffraction

Mineralogical composition was determined on both the bulk soil (soil sieved to 2 mm then ground to approximately 100 μm) and a fine fraction concentrated from the material sampled to decrease the quartz and feldspar contribution. The fine fraction was concentrated by suspending sediments in ethanol followed by sonication for 8 min (Perdrial et al., 2014). Particles remaining in suspension after 2 min were aspirated by pipette and air-dried prior to analysis. Using Stokes law we estimated the size of this fine fraction to be <30 μm. Approximately 0.2 g of each material was deposited on a glass slide and analyzed using a Rigaku MiniFlexII equipped with a Cu tube and scanned in 0.02° increments at $1^\circ\ \text{min}^{-1}$. Quantitative phase analysis was performed using the Rietveld module included in the X'Pert HighScore Plus software. After qualitative characterization of the mineralogy, phase mixtures were extracted from the literature as well as the AMCSD and COD databases (Downs and Hall-Wallace, 2003; Gražulis et al., 2009, 2011) and were modeled for scale factor, preferred orientation and peak shape (including March-Dollase factor).

RESULTS

Lithologic and Bulk Chemical Composition

Visual examination with a hand lens of gravels collected from the soil pits revealed a broad range of sources to the glacial till at SR and HB while gravels at WN reflected the local bedrock source. At SR, multiple lithologies, including phyllite, calcareous granulite, and mica schist are present in the Waits River Formation, the local bedrock underlying the study catchment (Hall, 1959); these lithologies contributed 23, 21, and 13% of the gravels examined, summing to a total of 57%. Granite containing both biotite and muscovite, distinctive to the New Hampshire magma series was the most common erratic lithology, contributing 23% of the gravels. Other lithologies present at 2 to 7% each included amphibolite, quartzite, calc-silicate granulite, felsite, and vein quartz. Calcium bearing minerals expected from these local bedrock units include calcite, plagioclase and hornblende, with minor to trace amounts of actinolite, epidote, clinozoisite, apatite, sphene, and grossular (Hall, 1959).

At HB, Bailey et al. (2003) reported that 68% of the gravels were from an erratic granodiorite found to the northwest of the study catchments while the mica schist of the local bedrock accounted for only 14%. Other lithologies contributing 4% or less included pegmatite, diabase, amphibolite, biotite granite, calc-silicate granulite, and quartzite. Calcium bearing minerals expected from the granodiorite and schist, based on local bedrock analyses, include plagioclase with minor to trace amounts of actinolite, epidote, clinozoisite, apatite, sphene and grossular (Englund, 1976).

In contrast to SR and HB, the lithologic composition of gravel at WN was relatively simple, including only sandstone and conglomerate at 55 and 45% each, respectively. Both lithologies are typical of the local bedrock and are dominated by quartz. Calcium bearing phases are not present in major amounts, with only trace amounts of plagioclase, calcite, and apatite reported (Ver Straeten, 2013; Gale, 1985).

Total elemental analysis revealed a wide range in soil Ca concentrations, from a low of 6.5 mmol kg^{-1} (0.04% CaO) in the WN Cd horizon to a relatively high 234 mmol kg^{-1} (1.31% CaO) in the SR Bw horizon (Table 2). Mg was also the most concentrated at SR while Si was most concentrated in the quartz-rich WN soil. Testing in a pressure calcimeter (detection limit 0.1% calcite equivalent) suggested that carbonate minerals were not present in any of the samples (data not included). Carbon in these soils is expected to be primarily associated with organic matter, typically composed of about 50% carbon, and was highest in the HB Bhs (spodic) horizon and lowest in the C horizon at WN. Analyzed oxides summed between 94 and 99.9%. The remainder between the sum of element oxide concentrations and 100% is likely due to structural water in phyllosilicates and amphiboles.

Table 2. Bulk elemental composition of soil samples expressed as oxides, mass percentage. Sites are Sleepers River Research Watershed 9 (SR) in northern Vermont, Hubbard Brook Experimental Forest (HB) in central New Hampshire, and Winnisook watershed (WN) in southeastern New York.

	SR	HB	WN
		%	
Al_2O_3	11.39	8.24	4.71
CaO	1.31	0.64	0.04
Fe_2O_3	4.19	3.00	2.41
K_2O	1.62	1.51	1.02
MgO	1.44	0.27	0.55
MnO	0.11	0.04	0.06
Na_2O	1.71	1.45	0.08
P_2O_5	0.10	0.11	0.04
SiO_2	69.98	71.05	90.25
OM	1.80	10.43	0.23
SrO	0.02	0.01	0.00
TiO_2	0.73	0.40	0.49
ZrO_2	0.04	0.03	0.03
Total	94.43	97.18	99.92

Determination of Mineral Identity by EPMA

Mineral identification of the clusters from the five-element EPMA mapping was based on point counts from the SR sample. These 30 initial EDS point counts provided multi-elemental analyses consistent with the Ca-bearing minerals actinolite, apatite, epidote/clinozoisite, hornblende and plagioclase, and non-Ca-bearing quartz, orthoclase, muscovite, biotite and possibly chlorite. All these Ca-bearing minerals were identified in the full SR map (Fig. 2a) and to verify this initial classification we used two approaches: (i) examination with a petrographic microscope and (ii) further EDS point counts. A number of larger grains in the SR sample (~0.25–1.0 mm diameter) were examined under normal and cross-polarized light, confirming the mapping of actinolite, clinozoisite, hornblende, plagioclase, muscovite and orthoclase. No initial identification based on the elemental analysis was contradicted. This examination under low-power magnification also made it clear that many grains were mixtures of minerals or small 'rocks', discussed below. Further point counts using SEM of smaller grains confirmed that we correctly assigned clusters for actinolite, clinozoisite/epidote, hornblende and plagioclase. We also found a grouping of four high-Ca (27% Ca) pixels (the minimum cluster size used was six pixels) that we identified as grossular garnet, which accounted for <0.1% of the total Ca. A few point counts were also collected for the HB and WN samples and confirmed apatite in the latter and actinolite, epidote and hornblende in HB. One small high-Ca grain measured in the HB sample matched diopside composition but it only occupied a few pixels and did not separate from other high-Ca minerals in the cluster analysis (and was an insignificant fraction of the total Ca). Overall, the mineral mapping was successful but some questions remained.

Additional SEM/EDS elemental mapping and point counts were used for four purposes: (i) to determine the full elemental composition of some remaining unidentified or tentatively identified Ca-bearing minerals, (ii) to determine the nature of the pixels grouped as 'edge' (difficult to identify because of low elemental counts), (iii) to examine weathered minerals, and (iv) to determine the mineral composition in fine-grained rock fragments. Most of our maps addressed more than one of these objectives. Eight examples are given below.

In the HB Bhs horizon, actinolite and epidote were tentatively identified via EPMA cluster analysis but did not fit perfectly with the elemental analyses. Use of SEM/EDS confirmed the presence of both (Fig. 3 and 4). The edge of large grains tended to have a few pixels identified as a different Ca-bearing mineral (e.g., the actinolite in the left portion of Fig. 3a). Edge pixels, identified as such, were also evident around the smaller grains of quartz and plagioclase in both EPMA maps. A somewhat weathered epidote/actinolite grain (Fig. 3c) was relatively well mapped by EPMA, although a number of the actinolite edge pixels were identified as hornblende. All Ca-bearing mineral phases were identified. The coarser scale EPMA maps for both areas correctly identified pla-

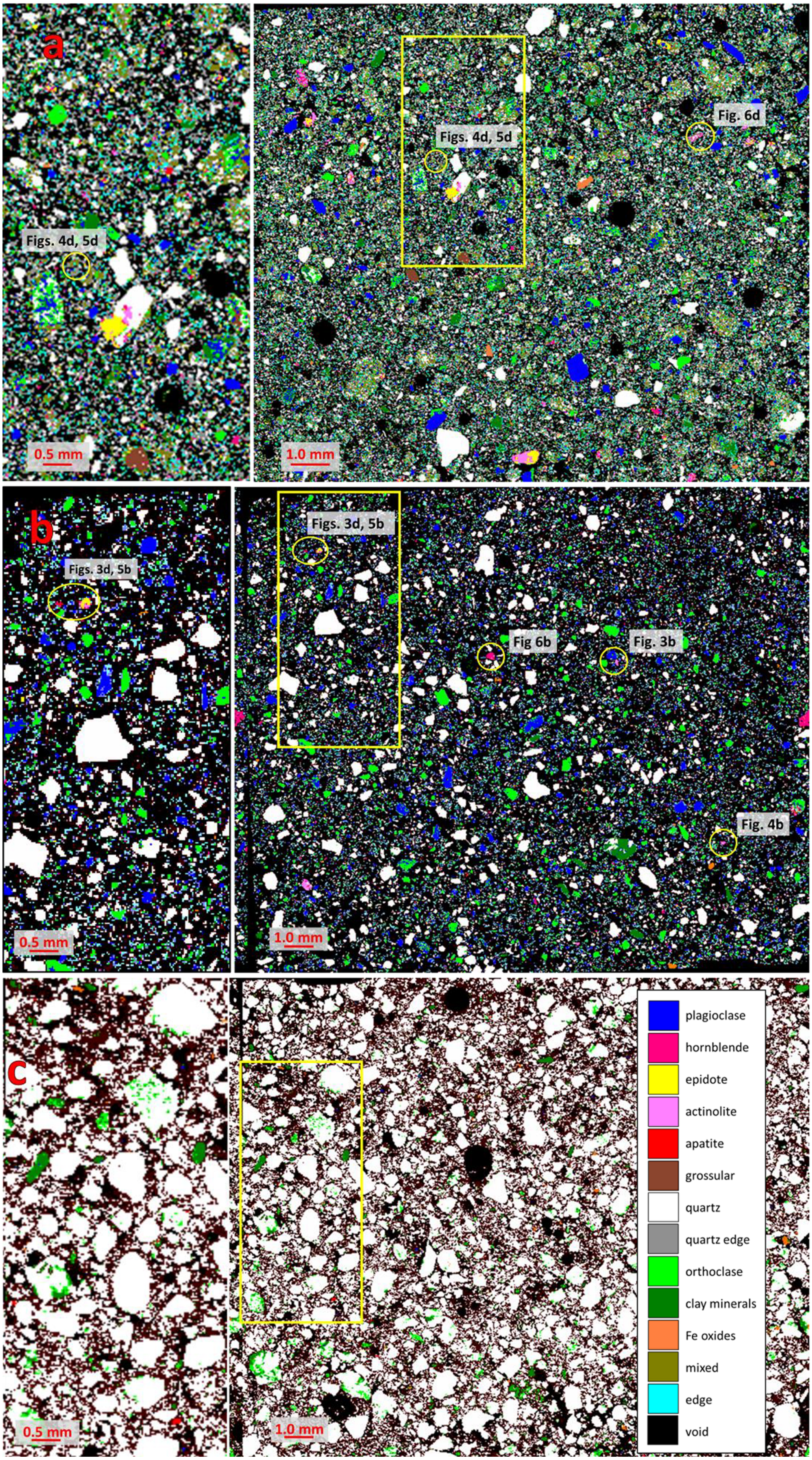

Fig. 2. Mineral maps of the full slide (right) and enlarged area shown in the yellow box (left) for (a) Sleepers River, (b) Hubbard Brook, and (c) Winnisook. The yellow circles identify areas shown at higher magnification in the subsequent figures.

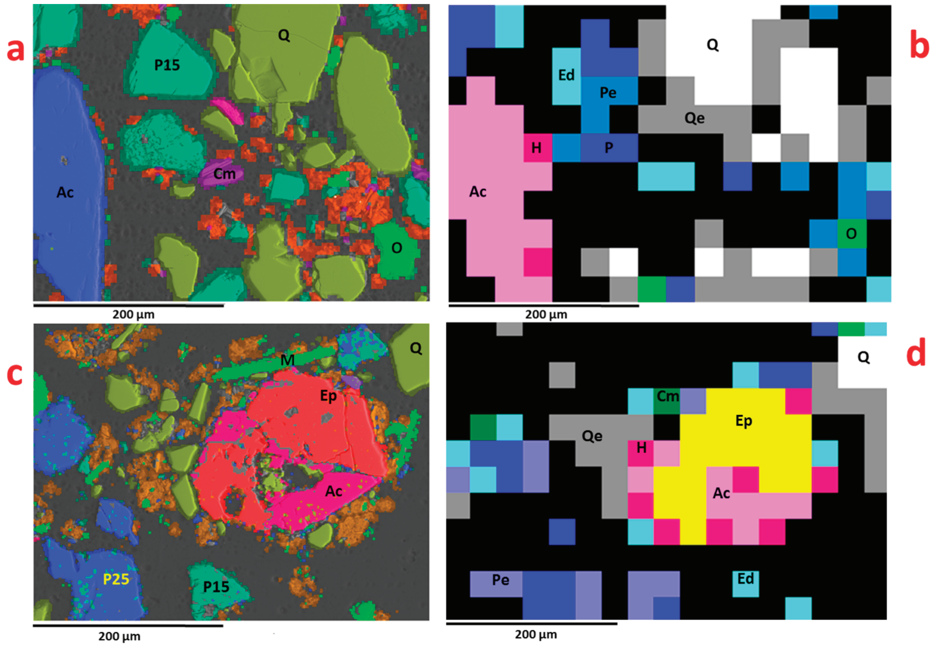

Fig. 3. Mineral identification from fine scale SEM/EDS (left) and 30-µm pixel EPMA (right) in two areas of the Hubbard Brook sample, showing largely correct identification of Ca-bearing minerals. The locations of these minerals in the larger EPMA map are shown in Fig. 2b. Mineral abbreviations are Ac, actinolite; Cm, clay minerals; Ed, edge; Ep, epidote; H, hornblende; M, muscovite; O, orthoclase; Q, quartz; Qe, quartz edge; P, P5, P15, P25, plagioclase unspecified, An5, An15, An25; Pe, plagioclase edge. The diffuse orange-brown areas in (a) and (c) are likely amorphous organometallic complexes (i.e., spodic material).

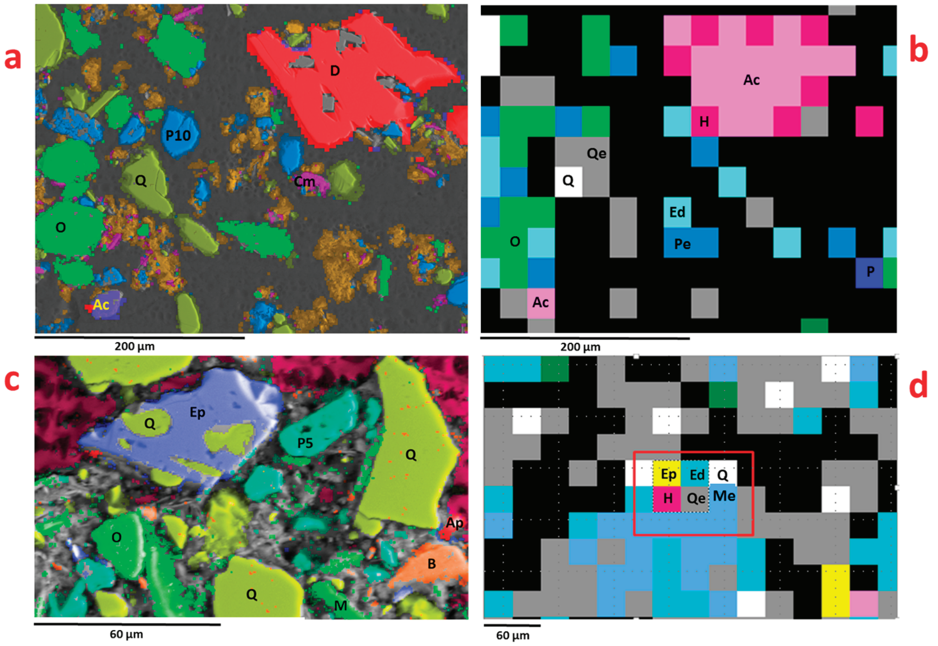

Fig. 4. Mineral identification from fine scale SEM/EDS (left) and 30-µm pixel EPMA (right) in one area each from the Hubbard Brook sample (a, b) and the Sleepers River sample (c, d). These EPMA maps (b, d) are examples of challenges to correct identification of Ca-bearing minerals. Diopside, a minor component of the HB sample (a), was identified as actinolite (b). Epidote with quartz inclusions in the SR sample (c) was only partially identified as epidote (d). Mineral abbreviations are Ac, actinolite; Ap, apatite; B, biotite; Cm, clay minerals; D, diopside; Ed, edge; Ep, epidote; H, hornblende; M, muscovite; Me, mixed/edge; O, orthoclase; Q, quartz; Qe, quartz edge; P, P5, P10, plagioclase unspecified, An5, An10; Pe, plagioclase edge.

gioclase, orthoclase, and quartz. Small clay mineral particles were identified in one area (Fig. 3d) but not the other (Fig. 3b). Both SEM/EDS maps showed what were likely spodic materials (amorphous organometallic complexes) between the mineral grains but the elemental counts were low and these areas were classified as void space. These two scans showed good identification of Ca-bearing minerals and relatively good classification of edge pixels.

We also found locations where our tentative identification was challenged (Fig. 4). In the HB sample, a 0.15 mm grain assigned to actinolite was found to have 14.8% Ca with SEM/EDS finer scale mapping and an overall formula closer to the ideal for diopside than actinolite (Fig. 4a). In the SR sample, a small grain (~0.05 mm) of what appears to be a low-Ca (5.5%) epidote mineral with quartz inclusions was initially assigned to hornblende and unknown (changed to epidote, Fig. 4d). Because this grain spans less than two pixels in the EPMA map and has inclusions, edge effects obviously influenced the EPMA results. In this same sample, we found a small (~5 µm) grain of apatite with SEM/EDS (right hand edge of Fig. 4c). This is the only instance of a 'missed' high-Ca mineral that we have found in our SEM/EDS mapping. Sphene ($TiCaSiO_5$) was found via SEM/EDS in two locations in the SR sample (not shown) and one grain in the HB horizon (Fig. 5a). Because of its high Ca content, it was clustered with apatite, and hornblende at the edges (Fig. 5b). The lack of Ti counts in the EPMA mapping made it difficult to separate this mineral. However, it was not widespread and all other apatite clusters that we examined were indeed apatite, including those mapped in the WN sample. These scans changed our mineral identification but the small size of the minerals meant that overall proportions of Ca-bearing minerals was not significantly affected.

Edge pixels were common in the two EPMA maps in Fig. 4 and in Fig. 5b, and were for the most part correctly associated with the minerals identified

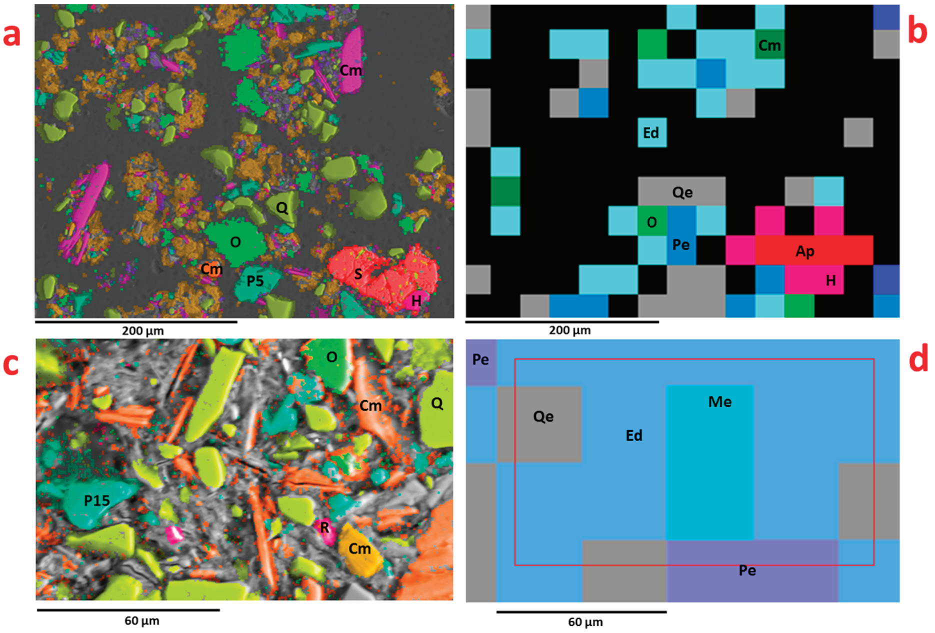

Fig. 5. Mineral identification from fine scale SEM/EDS (left) and 30-μm pixel EPMA (right) in one area each from the Hubbard Brook sample (a, b) and the Sleepers River sample (c, d) showing successes and challenges with small grains. In the HB sample, a grain of sphene (a) was identified as apatite and hornblende (b) but a smaller grain of hornblende was correctly mapped. The minerals smaller than 30 μm diameter in the SR samples (c) were identified as 'edge' components (d). Mineral abbreviations are Ap, apatite; Cm, clay minerals; Ed, edge; H, hornblende; Me, mixed/edge; O, orthoclase; Q, quartz; Qe, quartz edge; P5, P15, plagioclase An5, An15; Pe, plagioclase edge; R, rutile; S, sphene.

with the finer scale SEM/EDS mapping. We also examined a small area in the SR sample where all grains were smaller than the EPMA pixel size of 30 by 30 μm (Fig. 5c). The SEM/EDS map showed quartz, plagioclase AN15, orthoclase, clay minerals and rutile. The EPMA map (~3 by 4 pixels) showed only different edge phases. The presence of small plagioclase grains that were not clustered into either plagioclase or plagioclase edge (e.g., the 'P15' in Fig. 5c) suggests that this could be the source of the Ca attributed to edge (Table 3). These edge pixels clearly are problematic in fully mapping mineral content but do not appear to be masking the proportion of Ca-bearing minerals.

Grains that appeared somewhat weathered still allowed mineral identification by EPMA mapping. In the HB sample, a relatively large (~0.2 mm) weathered hornblende (confirmed with EDS point counts) was mostly mapped as hornblende (Fig. 6a and b). In the SR horizon, a large (~0.5 mm) grain was actually a rock fragment with actinolite, quartz and voids where more weatherable minerals were likely once found (Fig. 6c and d). This occurrence of mixed mineral assemblages was fairly common, especially in the SR sample. Identification of the individual minerals appeared to be possible when their sizes exceeded that of the EPMA pixel. The presence of voids and of smaller grain sizes made identification more problematic and resulted in a cluster assigned to 'mixed/edge' in this particular sample. A smaller pixel size could resolve this problem but would also lead to much longer analytical time. The ability to correctly map weathered minerals or mineral assemblages varied with the grain size.

Accounting of Soil Ca Content by EPMA Mineral Inventory

The EPMA maps showed clear differences in Ca intensity, corresponding to a range of Ca-bearing minerals (Fig. 2). Apatite was the only Ca-bearing mineral identified in all three samples and even though it occupied only 0.04% of the non-void pixels in the WN Cd, it accounted for 97.5% of the total Ca (Table 3). At the other two sites, apatite was present in similar amounts but accounted for <2% of the total Ca. The most common Ca-bearing mineral in the SR and HB samples was plagioclase (39% of the Ca at SR and 32% at HB). Hornblende contributed 15% and 8% of the total Ca at SR and HB, respectively. Actinolite and epidote minerals comprised <1% of the non-void space in soil thin sections at both sites but together contributed 28% of the total Ca at SR and 4% at HB (Table 3). A small amount of garnet (0.2% of non-void space) was found in the SR sample and amounted to a low contribution to the total Ca (4%). Calcite and dolomite were not found in any samples although both are present in lithologies contributing to soil parent material, and as bedrock at SR.

Overall, quartz dominated the mineral content at all sites, comprising 97% of the non-void space in the WN Cd horizon and about 51–63% in the other two samples (Table 3). Other non-Ca-bearing minerals included orthoclase, muscovite, biotite, and iron oxides. A group of pixels were lumped as "mixed". These were largely fine grained clastic rocks at WN. Pixels not identified in the SR and HB samples as any distinct mineral phase included a number of polymineralic fine grained crystalline rock fragments. Pixels lumped into the mixed category did not contribute a measurable amount of Ca (Table 3).

Summing together the Ca contributions from minerals determined by EPMA yielded a soil Ca content of 0.87, 0.45, and 0.01% at SR, HB, and WN, respectively. Salt extraction of these samples yielded measurable quantities of Ca at SR and HB, of 0.07 and 0.01%, respectively, while salt extractable Ca at WN was 0.001%. Summing mineral Ca and salt extractable Ca yielded a total soil Ca content of 0.94, 0.46, and 0.03% at SR, HB, and WN, respectively. This matched the bulk Ca concentration determined by lithium-borate fusion at SR and HB. Bulk Ca concentration at WN by lithium-borate fusion was very low at 0.03%, although this was higher than the concentration determined by mineral inventory (0.01%; Table 3).

Mineral Inventory from X-ray Diffraction

Quartz was the dominant mineral found by XRD at all three sites, contributing 56, 65, and 89% at SR, HB, and WN, respectively in bulk samples (Table 4). Quartz concentrations in

Table 3. Soil mineral content based on EPMA and contribution to soil Ca content, mass percentage. Sites are Sleepers River Research Watershed 9 (SR) in northern Vermont, Hubbard Brook Experimental Forest (HB) in central New Hampshire, and Winnisook watershed (WN) in southeastern New York.

	Soil mineral abundance			Mineral Ca	Contribution to soil Ca		
	SR	HB	WN	Ca	SR	HB	WN
	%						
Ca-bearing phases							
Plagioclase	11.79			3.29	0.39		0.00
Plagioclase		15.20		2.09		0.32	
Hornblende	1.71	0.89		8.60	0.15	0.08	0.00
Epidote	1.04	0.14		16.90	0.18	0.02	0.00
Actinolite	1.16	0.24		8.20	0.10	0.02	0.00
Apatite	0.06	0.02	0.03	38.60	0.02	0.01	0.01
Grossular garnet	0.42			9.99	0.04	0.00	0.00
Mixed			0.03	0.10	0.00	0.00	0.00003
Other phases							
Quartz	51.05	62.66	96.88				
Orthoclase	4.63	10.70	0.94				
Muscovite	0.95	1.36					
Biotite	3.96	1.38					
Fe-oxide	0.74	0.39	0.43				
Mixed	22.50	7.03	1.69				
Total from EPMA	100.00	100.00	100.00		0.87	0.45	0.01
Salt-extractable Ca					0.07	0.01	0.001
Ca EPMA plus salt extraction					0.94	0.46	0.01
Ca from Li-borate fusion					0.94	0.46	0.03

the less than 30 µm fraction were 54 to 62% of the concentrations measured in the bulk samples. Other non-Ca-bearing minerals detected were similar to those found by EPMA, including relatively abundant K-feldspar (anorthoclase) and muscovite. An Fe-bearing mica was found in all three samples and identified as an Fe-bearing chlorite. A trace of montmorillonite was detected at HB while an Fe-oxide, hematite, was detected at WN.

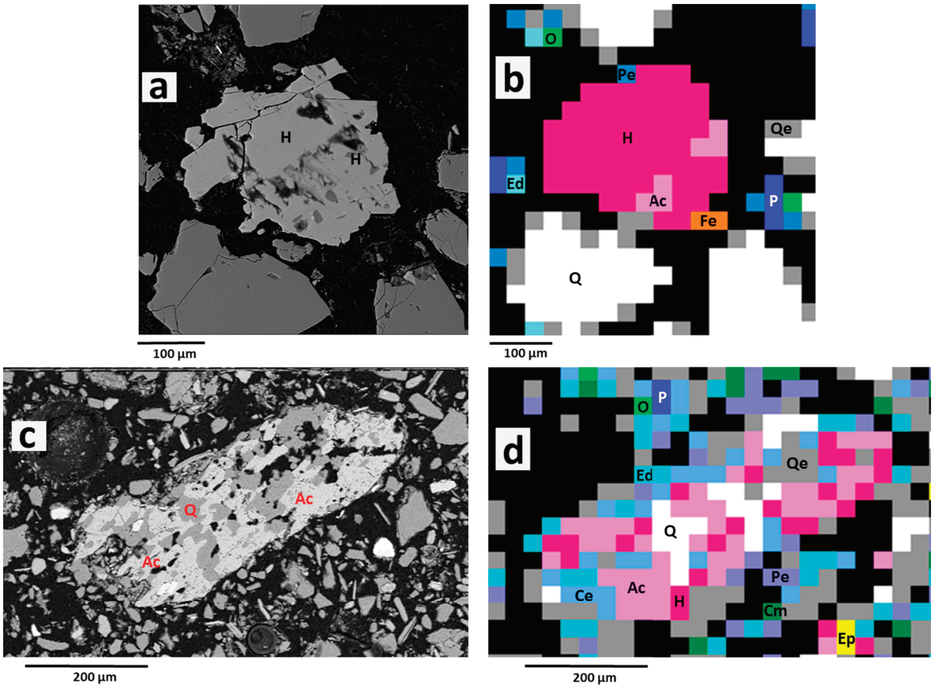

Fig. 6. Examples of small rocks from the Hubbard Brook sample (a, b) and the Sleepers River sample (c, d). SEM images on the left (a, c) show the fine scale of mineral assemblage and void space. Mineral identification is from elemental point counts. The 30-µm pixel EPMA mineral mapping on the right (b, d) shows relatively good success with identification. Mineral abbreviations are Ac, actinolite; Ce, conglomerate/edge; Cm, clay minerals; Ed, edge; Ep, epidote; Fe, iron oxide; H, hornblende; O, orthoclase; Q, quartz; Qe, quartz edge; P, plagioclase; Pe plagioclase edge.

Ca-bearing hornblende was detected by XRD in SR and HB, composing 2.9 and 0.6% of the bulk sample, respectively. Plagioclase feldspars were detected at both SR and HB. As plagioclase species determination is difficult by XRD, we chose to conservatively model the plagioclase as labradorite (50% An). Following this assumption, using EPMA measured plagioclase compositions (Table 3) such that Ca contributes 3.3% of labradorite's mass at SR, 2.1% of labradorite's mass at HB and 7% or hornblende's mass, we estimated Ca contribution from XRD-detected minerals at SR, HB and WN to be 0.90, 0.26, and 0.0%, respectively.

DISCUSSION

Determination of gravel lithology suggested that bedrock proximal to the sample locations was the dominant source of glacial till from which the soil was derived. At WN, where the study site is with-

Table 4. Soil mineral content from x-ray diffraction analysis of bulk soil and soil particles less than 30 µM. Sites are Sleepers River Research Watershed 9 (SR) in northern Vermont, Hubbard Brook Experimental Forest (HB) in central New Hampshire, and Winnisook watershed (WN) in southeastern New York.

	Soil mineral abundance					
	SR		HB		WN	
	Bulk	<30 µM	Bulk	<30 µM	Bulk	<30 µM
	%					
Ca-bearing phases						
Ca-plagioclase	21.1	11.7	10.5	26.0		
Hornblende	2.9	2.4	0.6			
Other phases						
Quartz	56.4	30.6	64.8	34.7	88.8	54.8
Anorthoclase	1.5	5.8	12.5	12.7		
Muscovite	13.1	35.4	8.6	20.0	8.1	34.4
Fe-chlorite	5.0	14.2	2.5	6.6	2.2	8.9
Montmorillonite			0.5			
Hematite					0.9	1.9
Total from XRD	100.0	100.1	100.0	100.0	100.0	100.0

in a relatively large area mapped as sandstone and conglomerate bedrock, these lithologies accounted for the entire sample. In contrast, at HB, where there is a contact between the local schist bedrock and a large granitic pluton just to the northwest, the erratic granite made up the majority of the sample. The SR sample was intermediate in representation of underlying and erratic lithologies. However, all three samples were consistent with a local derivation, similar to the results of Goldthwaite et al. (1951), and generalized into a wedge-shaped glacial till source area by Bailey and Hornbeck (1992).

With the source lithologies of the gravel as a guide, a list of likely Ca-bearing minerals to be found in the soil was generated, and largely agreed with the minerals found by EPMA. Using generalized mineral chemistry, along with specific mineral chemistry from SEM-EDS for solid-solution minerals, and a small contribution of non-mineral Ca indicated by salt extraction, we were able to account for the bulk Ca content of the soil samples determined by lithium-borate fusion. Thus, three methods, the gravel inventory, EPMA mineral inventory combined with non-mineral sources, and bulk chemical composition provide compatible results, lending confidence in our determination of the nature and concentration of Ca sources in these samples.

X-ray diffraction roughly agreed with EPMA for the identity and relative concentrations of major minerals present in the samples. For example, the relative prevalence of quartz at the three sites was in agreement and the concentrations at SR and HB were similar between the two methods. However quartz content at WN was significantly lower for XRD. X-ray diffraction failed to find most non-plagioclase Ca bearing minerals expected from lithologic composition and found by EPMA. Furthermore, while the concentration of soil Ca indicated by the XRD mineral inventory was close to that measured by lithium-borate fusion, an accurate estimation of Ca content based on XRD is virtually impossible due to the difficulty of determining the precise plagioclase species by XRD of complex mixtures.

While previous studies have demonstrated the utility of EPMA to identify specific minerals in soil thin sections and to determine the composition of soil particles (Bisdom et al., 1983; Kim et al., 2006; Brock-Hon and Morgenthaler, 2019), this may be the first application of EPMA as the central technique of determining a whole soil sample mineral inventory. There are a number of advantages to the EPMA method relative to other approaches used to quantify soil mineralogy, especially in situations where primary minerals are actively weathering. The modeling approaches that use bulk chemical composition are based on a particular set of minerals with particular elemental content. Results need to be validated when applied to different locales where both the mineralogy may differ along with the range of elemental percentages within similar minerals. It may also be possible to fit the elemental data with different combinations of a suite of minerals. Further, this approach will also be challenged by the presence of partially weathered minerals that have less than their ideal concentration of some elements. Bulk XRD, as shown here, can quantify the major mineral phases but has difficulty showing minor phases that may be important contributors to overall elemental composition, such as apatite. Synchrotron-based micro-XRD can provide unequivocal soil mineral identification down to the micrometer scale. Scaling up to a sample size suitable for characterizing a soil horizon is challenging both because of the beam-time needed for such mapping and the data processing needed to interpret the XRD patterns for each pixel. In addition, any XRD method may have difficulty identifying partially weathered minerals that have lost some of their crystallographic symmetry. EPMA mineral phase mapping is a viable approach because it can automate elemental mapping of a relatively large sample, and after some intensive effort in associating these results with mineral phases, result in relatively easy quantification of mineral phase percentages and the elemental contributions of these individual minerals. There are a number of challenges, detailed in our results and discussed further below. While EPMA is not able to directly identify mineralogy similar to XRD, specific minerals can be confirmed by having a database of local bedrock mineralogy and elemental composition. Partially weathered minerals can be identified by being within a range of the ideal composition (e.g., Fig. 6b). SEM EDS point counts of a suite of elements, beyond the five measured by the EPMA maps, provide further confirmation of mineral phases.

The biggest challenge we found with EPMA mineral identification was in the edge pixels. When mapping rock samples, pixels along the boundary of two minerals can usually be assigned to each mineral proportionally because their elemental composition will reflect a simple average of the two phases. With soil particles, much of the edge is between a mineral and void space. In many instances, it is clear that the pixel is a certain percentage of the ideal elemental concentration for a particular, common mineral. For example, a pixel could be ~60% of the Si, Al and Ca concentration as that of the plagioclase elsewhere in the same map or 55% of the Si in quartz along with minimal amounts of Al, Ca and Fe. In these cases, we would assign the estimated percent of the mineral in the pixel to either plagioclase or quartz. There are, however, pixels in which the percentages cannot be easily assigned to a known mineral, likely because of overlap within the pixel of more than one mineral phase. The soils we studied were of relatively coarse texture, as they were either sandy loams or loams (Table 1), and most of the soils in the upland forest of the northeastern USA and eastern Canada are similar in texture. Between 59 and 75% of the particles were coarse silt and sand, and should have been identifiable within one 30- by 30-µm pixel. We found no evidence of different Ca-bearing mineral phases in the finer fraction in either the EPMA mapping in two 0.5 by 0.5 mm areas of the SR sample using 10 by 10 µm pixels or in any of the SEM EDS finer scale mapping. Our soils were low in clay-sized particles (6–10%) and in secondary clay minerals. In finer textured soils, this edge problem would be more severe and a smaller pixel size for the map might be needed. This would either involve a longer analysis time for a similar sized map or, instead, choosing a smaller map size.

A second challenge with EPMA mineral identification was the unanticipated presence of small fine-grained rocks in which some of the individual minerals were close to our 30-µm pixel size. A good example of this is the ~0.250 by 0.750 mm grain from the SR sample shown in Fig. 6c. A few point counts identified quartz and actinolite (Fig. 6c), while the EPMA mapping also included hornblende and edge (Fig. 6d). In addition, there appears to be void space, especially in the upper right of the grain. The missing mineral here would likely be calcite and the rock itself calcareous granulite, a common lithology of the Waits River Formation, the local bedrock at the study site. Edge pixels in this grain are either at the boundary of two minerals or may include some void space. While EPMA may have mapped the minerals within in this rock sufficiently well, other such sand or silt sized rock fragments had even finer grained components (e.g., the ~0.5 by 1.0 mm rock in the 10 by 10 µm pixel EPMA map; Supplemental Fig. S2). While much of this grain was mapped as either quartz, plagioclase or orthoclase, a section near the top and bottom was simply mapped as 'conglomerate/edge'). This may be a combined factor of small mineral crystal size and greater weathering in these two areas.

Since their first commercialization in 1956 (Heath and Taylor, 2015), electron microprobes have become widespread across the world and EPMA facilities can be found in many large geosciences departments and facilities (Robinson, 2019). This renders them more accessible than other advanced analytical approaches, in particular those requiring synchrotron radiation. Protocols for soil samples will be identical to those for more consolidated materials.

Determination of quantitative contributions of specific mineral species to soil Ca supply has the potential to improve estimates of mineral weathering rates in nutrient cycling and critical loads models. At these three sites, spanning a range of bulk soil Ca content and lithologic source of glacial till from which the soils were derived, most of the Ca source minerals were at low concentrations. As our samples were from mid B horizon to the C horizon, it is plausible that even lower concentrations would have been measured, or some of these minerals may not have been detectable in shallower horizons, particularly the forest floor and upper B horizons, where most root activity is present. Future applications of the EPMA mapping technique may concentrate on determining abundance depth profiles of Ca bearing minerals, to determine what portion of the soil profile minerals are depleted from versus those portions of the profile where active mineral weathering may be occurring.

CONCLUSIONS

Mapping of soil mineralogy and inventory of Ca sources by EPMA gave quantitative results consistent with bulk Ca composition and with mineral phases expected from glacial till sources at each sample site. This method provides better detection of Ca minerals at low concentration than XRD and provides a more definitive identification than interpretation of bulk chemistry or sequential extraction procedures. Studies to quantify Ca weathering rates in soil and to evaluate potential of recovery of soil Ca supply following disturbance, such as by acid deposition, will benefit from application of this technique in soil studies.

ACKNOWLEDGMENTS

This study was partially funded by a grant from the Northeastern States Research Cooperative. The Sleepers River Research Watershed is owned by the State of Vermont and operated by the WEBB Program, US Geological Survey. Sampling at Sleepers River was facilitated by James Shanley, USGS. Hubbard Brook Experimental Forest is owned and operated by the USDA Forest Service, Northern Research Station, Newtown Square, PA. Permission to sample at Winnisook was granted by the Winnisook Club and was facilitated by Gregory Lawrence, USGS.

SUPPLEMENTAL MATERIAL

Supplemental material is available with the online version of this article. The supplement contains Table S1, Rules used for initial mineral classification; Fig. S1, Examples of geometrically corrected scan intensity; and Fig. S2, Finer scale EPMA map of a 5 by 5 mm section of the SR sample showing the resolution with a 10 by 10 µm pixel size, an enlargement of the EPMA RGB image showing detail in the 0.5 by 1.0 mm multi-mineral soil particle, and an SEM image of the same multi-mineral particle.

REFERENCES

Bailey, S.W., D.C. Buso, and G.E. Likens. 2003. Implications of sodium mass balance for interpreting the calcium cycle of a forested ecosystem. Ecology 84:471–484. doi:10.1890/0012-9658(2003)084[0471:IOSMBF]2.0.CO;2

Bailey, S.W., and J.W. Hornbeck. 1992. Lithologic composition and rock weathering potential of forested, glacial-till soils. Res. Pap. NE-662. USDA

Forest Service, Northeastern Forest Experiment Station, Radnor, PA.

Bailey, S.W., J.W. Hornbeck, C.T. Driscoll, and H.E. Gaudette. 1996. Calcium inputs and transport in a base-poor forest ecosystem as interpreted by Sr isotopes. Water Resour. Res. 32:707–719. doi:10.1029/95WR03642

Bailey, S.W., S.B. Horsley, and R.P. Long. 2005. Thirty years of change in forest soils of the Allegheny Plateau, Pennsylvania. Soil Sci. Soc. Am. J. 69:681–690. doi:10.2136/sssaj2004.0057

Biehl, L., and D. Landgrebe. 2002. MultiSpec—a tool for multispectral–hyperspectral image data analysis. Comput. Geosci. 28:1153–1159. doi:10.1016/S0098-3004(02)00033-X

Binkley, D., and D. Richter. 1987. Nutrient cycles and H+ budgets of forest ecosystems. Adv. Ecol. Res 16:1–51. doi:10.1016/S0065-2504(08)60086-0

Bisdom, E.B.A., S. Henstra, H.W. Werner, P.R. Boudewijn, W.F. Knippenberg, H.A.M. De Grefte, J.M. Gourgout, and H.N. Migeon. 1983. Quantitative analysis of trace and major elements in thin sections of soils with the secondary ion microscope (Cameca). Geoderma 30:117–134. doi:10.1016/0016-7061(83)90060-5

Blume, L.J., B.A. Schumacher, P.W. Schaffer, K.A. Cappo, M.L. Papp, R.D. van Remortel, D.S. Coffey, M.G. Johnson, and D.J. Chaloud. 1990. Handbook of methods for acid deposition studies laboratory analyses for soil chemistry. EPA/600/4-90/023. UPA Environmental Monitoring Systems Laboratory, Las Vegas, NV.

Brantley, S.L. 2008. Kinetics of mineral dissolution. In: S.L. Brantley, S. Kubicki, and A. White, editors, Kinetics of water-rock interaction. Springer, New York. p. 151–210. doi:10.1007/978-0-387-73563-4_5

Brock-Hon, A.L., and S. Morgenthaler. 2019. Investigation of limestone and dolomite clast alteration in petrocalcic horizons, southern Nevada, USA. Geoderma 342:42–54. doi:10.1016/j.geoderma.2019.02.004

Casetou-Gustafson, S., C. Akselsson, S. Hillier, and B.A. Olsson. 2019. The importance of mineral determinations to PROFILE base cation weathering release rates: A case study. Biogeosciences 16:1903–1920. doi:10.5194/bg-16-1903-2019

Cleveland, W.S., E. Grosse, and W.M. Shyu. 1992. Local regression models. In: J.M. Chambers and T.J. Hastie, editors, Statistical models in S. Chapman and Hall/CRC Press, New York. p. 309–376.

Day, P.R. 1965. Particle fractionation and particle size analysis. In: C.A. Black, editor, Methods of soil analysis, Part 1. ASA, Madison, WI. p. 545–567.

Deer, W.A., R.A. Howie, and J. Zussman. 2013. An introduction to the rock-forming minerals. Third Ed. The Mineralogical Society, London.

Downs, R.T., and M. Hall-Wallace. 2003. The American mineralogist crystal structure database. Am. Mineral. 88:247–250.

Englund, E.J. 1976. The bedrock geology of the Holderness Quadrangle. State of New Hampshire Department of Resources and Economic Development, Concord, NH.

Federer, C.A., J.W. Hornbeck, L.M. Tritton, C.W. Martin, R.S. Pierce, and C.T. Smith. 1989. Long-term depletion of calcium and other nutrients in eastern US forests. Environ. Manage. 13:593–601. doi:10.1007/BF01874965

Fernandez, I.J., L.E. Rustad, S.A. Norton, J.S. Kahl, and B.J. Cosby. 2003. Experimental acidification causes soil base-cation depletion at the Bear Brook Watershed in Maine. Soil Sci. Soc. Am. J. 67:1909. doi:10.2136/sssaj2003.1909

Futter, M.N., J. Klaminder, R.W. Lucas, H. Laudon, and S.J. Köhler. 2012. Uncertainty in silicate mineral weathering rate estimates: Source partitioning and policy implications. Environ. Res. Lett. 7:024025. doi:10.1088/1748-9326/7/2/024025

Gale, P.E. 1985. Diagenesis of the middle to upper Devonian Catskill facies sandstones in southeastern New York State. Harvard University, Cambridge, MA.

Goldthwaite, J.W., L. Goldthwaite, and R.P. Goldthwaite. 1951. The geology of New Hampshire. Part 1. Surficial geology. New Hampshire Department of Resources and Economic Development, Concord, NH.

Gražulis, S., D. Chateigner, R.T. Downs, A. Yokochi, M. Quirós, L. Lutterotti, E. Manakova, J. Butkus, P. Moeck, and A. LeBail. 2009. Crystallography open database–an open-access collection of crystal structures. J. Appl. Cryst. 42:726–729. doi:10.1107/S0021889809016690

Gražulis, S., A. Daškevič, A. Merkys, D. Chateigner, L. Lutterotti, M. Quirós, N.R. Serebryanaya, P. Moeck, R.T. Downs, and A. LeBail. 2011. Crystallography open database: An open-access collection of crystal structures and platform for world-wide collaboration. Nucleic Acids Res. 40:D420–D427. doi:10.1093/nar/gkr900

Hall, L.M. 1959. The geology of the St. Johnsbury Quadrangle, Vermont and New Hampshire. Vermont Development Commission, Montpelier, VT.

Heath, J., and N. Taylor, editors. 2015. Electron probe microanalysis. John Wiley & Sons, Chichester, UK.

Johnson, C.E., J.J. Ruiz-Méndez, and G.B. Lawrence. 2000. Forest soil chemistry and terrain attributes in a Catskills watershed. Soil Sci. Soc. Am. J. 64:1804–1814. doi:10.2136/sssaj2000.6451804x

Kim, H., H. Hwang, and C. Ro. 2006. Single-particle characterization of soil samples collected at various arid areas of China, using low-Z particle electron probe x-ray microanalysis. Spectrochim. Acta B At. Spectrosc. 61:393–399. doi:10.1016/j.sab.2006.01.012

Kolka, R.K., D.F. Grigal, and E.A. Nater. 1996. Forest soil mineral weathering rates: Use of multiple approaches. Geoderma 73:1–21. doi:10.1016/0016-7061(96)00037-7

Lawrence, G.B., P.W. Hazlett, I.J. Fernandez, R. Ouimet, S.W. Bailey, W.C. Shortle, K.T. Smith, and M.R. Antidormi. 2015. Declining acidic deposition begins reversal of forest-soil acidification in the northeastern US and eastern Canada. Environ. Sci. Technol. 49:13103–13111. doi:10.1021/acs.est.5b02904

Likens, G.E., C.T. Driscoll, and D.C. Buso. 1996. Long-term effects of acid rain: Response and recovery of a forest ecosystem. Science 172:244–246. doi:10.1126/science.272.5259.244

Lydon, J.W. 2005. The measurement of the modal mineralogy of rocks from SEM imagery: The use of multispec and imageJ freeware. Open File 4941. Geological Survey of Canada. doi:10.4095/220706

McHale, M.R., D.A. Burns, J. Siemion, and M.R. Antidormi. 2017. The response of soil and stream chemistry to decreases in acid deposition in the Catskill Mountains, New York, USA. Environ. Pollut. 229:607–620. doi:10.1016/j.envpol.2017.06.001

Palmer, S.M., C.T. Driscoll, and C.E. Johnson. 2004. Long-term trends in soil solution and stream water chemistry at the Hubbard Brook Experimental Forest: Relationship with landscape position. Biogeochemistry 68:51–70. doi:10.1023/B:BIOG.0000025741.88474.0d

Pardo, L.H. 2010. Approaches for estimating critical loads of N and S deposition for forest ecosystems on US federal lands. Gen. Tech. Rep. NRS-71. USDA Forest Service, Northern Research Station, Newtown Square, PA. doi:10.2737/NRS-GTR-71

Park, B.B., R.D. Yanai, T.J. Fahey, S.W. Bailey, T.G. Siccama, J.B. Shanley, and N.L. Cleavitt. 2008. Fine root dynamics and forest production across a calcium gradient in northern hardwood and conifer ecosystems. Ecosystems 11:325–341. doi:10.1007/s10021-008-9126-3

Perdrial, N., A. Thompson, P.A. O'Day, C.I. Steefel, and J. Chorover. 2014. Mineral transformation controls speciation and pore-fluid transmission of contaminants in waste-weathered Hanford sediments. Geochim. Cosmochim. Acta 141:487–507. doi:10.1016/j.gca.2014.06.022

R Core Team. 2013. R: A language and environment for statistical computing". R Foundation for Statistical Computing, Vienna, Austria.

Robinson, B. 2019. EPMA and SEM facilities, World Wide. https://epmalab.uoregon.edu/otherlab.htm (accessed 18 Sept. 2019).

Soil Survey Staff. 2014. Keys to soil taxonomy, 12th Ed. USDA, Natural Resources Conservation Service, Washington, DC.

Sverdrup, H., and P. Warfvinge. 1993. Calculating field weathering rates using a mechanistic geochemical model PROFILE. Appl. Geochem. 8:273–283. doi:10.1016/0883-2927(93)90042-F

Vadeboncoeur, M.A., S.P. Hamburg, R.D. Yanai, and J.D. Blum. 2014. Rates of sustainable forest harvest depend on rotation length and weathering of soil minerals. For. Ecol. Manage. 318:194–205. doi:10.1016/j.foreco.2014.01.012

Velbel, M.A., and J.R. Price. 2007. Solute geochemical mass-balances and mineral weathering rates in small watersheds: Methodology, recent advances, and future directions. Appl. Geochem. 22:1682–1700. doi:10.1016/j.apgeochem.2007.03.029

Ver Straeten, C.A. 2013. Beneath it all: Bedrock geology of the Catskill Mountains and implications of its weathering. Ann. N. Y. Acad. Sci. 1298:1–29.